The Journal of Chemical Physics ARTICLE scitation.org/journal/jcp

Mid-IR quantum cascade laser spectroscopy to resolve lipid dynamics during the photocycle of bacteriorhodopsin

Cite as: J. Chem. Phys. 158, 154202 (2023); doi: 10.1063/5.0139808
Submitted: 23 December 2022 • Accepted: 3 April 2023 •
Published Online: 19 April 2023

Paul Stritt, Michael Jawurek, and Karin Hauser[a)]

AFFILIATIONS

Department of Chemistry, University of Konstanz, 78457 Konstanz, Germany

[a)] Author to whom correspondence should be addressed: karin.hauser@uni-konstanz.de

ABSTRACT

Membranes are crucial for the functionality of membrane proteins in several cellular processes. Time-resolved infrared (IR) spectroscopy enables the investigation of interaction-induced dynamics of the protein and the lipid membrane. The photoreceptor and proton pump bacteriorhodopsin (BR) was reconstituted into liposomes, mimicking the native purple membrane. By utilization of deuterated lipid alkyl chains, corresponding vibrational modes are frequency-shifted into a spectrally silent window that allows us to monitor lipid dynamics during the photoreaction of BR. Our home-built quantum cascade laser (QCL)-based IR spectrometer covers all relevant spectral regions to detect both lipid and protein vibrational modes. QCL-probed transients at single wavenumbers are compared with the previously performed step-scan Fourier-transform IR measurements. The absorbance changes of the lipids could be resolved by QCL-measurements with a much better signal-to-noise ratio and with nanosecond time resolution. We found a correlation of the lipid dynamics with the protonation dynamics in the M intermediate. QCL spectroscopy extends the study of the protein's photocycle toward dynamics of the interacting membrane.

INTRODUCTION

Membrane proteins are essential for carrying out biological processes within a living cell. They enable the cell to communicate with its intracellular and extracellular environment as well as regulate the signal and transport processes across the membrane barrier. The lipid membrane has a critical role in the localization of membrane proteins and, furthermore, is pivotal in the protein's overall functionality. Microbial rhodopsins, in particular, bacteriorhodopsin (BR), are adequate model systems for the study of protein–membrane interactions. Since that time it was reported as a new photoreceptor membrane,[1] the light-driven proton pump BR has been extensively studied using various techniques[2–5] and utilized in several applications.[6] The membrane protein BR occurs as trimers in the native purple membrane of *Halobacterium salinarium*, which is composed of polar and neutral lipids.[7] BR consists of seven transmembrane α-helices with the retinal chromophore linked to the lysine residue by a protonated Schiff base. After light excitation, isomerization of the retinal from the all-*trans* to 13-*cis* state occurs, followed by the thermal reisomerization back to the initial all-*trans* configuration.[8] Thereby, BR passes through a series of different intermediate steps. K, L, M, N, and O are photocycle intermediates[4,9,10] and describe the state of the protein and the chromophore, including individual steps of the proton translocation. After photoisomerization, the first proton transfer step occurs from the retinal Schiff base to the primary proton acceptor Asp85. Subsequent to the Asp85 protonation, a proton release group provides a proton to the extracellular side. Thereafter, the Schiff base gets reprotonated[11] from the donor Asp96 followed by a proton uptaken from the cytoplasmic side.[12] This accessibility change of the Schiff base from the extracellular to the cytoplasmic channel is referred to as switch.[8] The switch happens during the M intermediate, accompanied by a large conformational change in the M/N intermediate.[12] In addition, the first proton transfer step corresponds to the M intermediate[13] and is reported to occur about 300–400 μs after photoexcitation.[14,15] Since M is the only intermediate with a

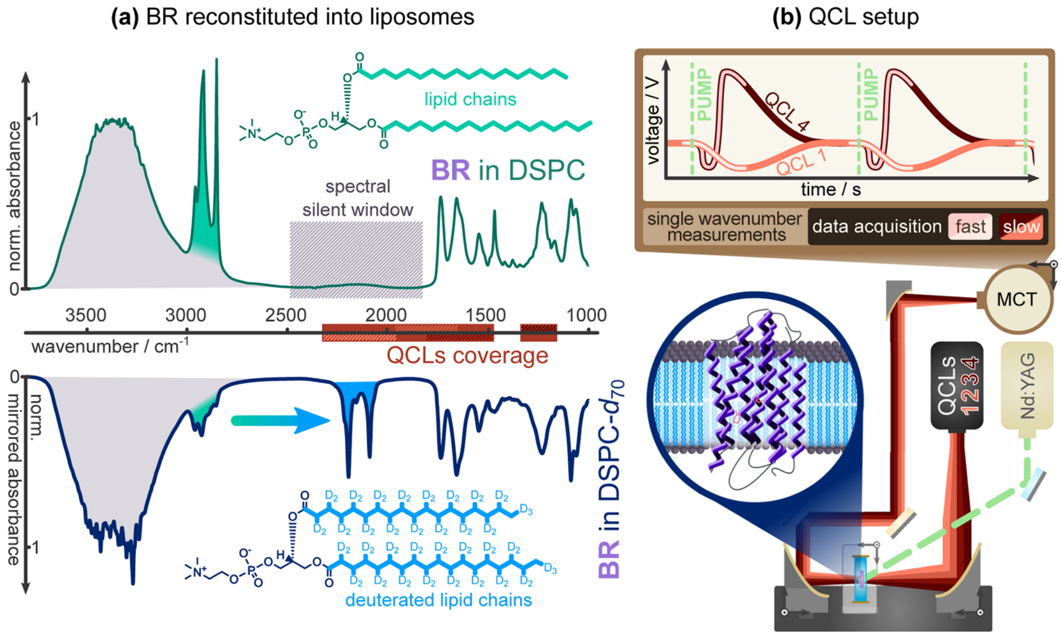

FIG. 1. (a) The absorption spectrum of BR reconstituted into liposomes composed of DSPC (top, green) is shown with its lipid chain bands overlaying with the water band at ~3400 cm^{-1} (gray). The spectral silent window is marked in this spectrum. For straight comparability, the y-axis of the absorption spectrum of BR reconstituted into deuterated liposomes with DSPC-d_{70} (bottom, blue) is represented in mirrored form. DSPC-d_{70} lipids differ from DSPC only in their fully deuterated lipid chains. Therefore, the bands of the lipid chains are shifted into a spectral silent window, which is covered by the emission of the QCLs (marked along the x-axis). (b) The QCL spectrometer setup is schematically illustrated in a reduced version with the four probe laser heads, the pump laser for photoexcitation (Nd:YAG), the MCT detector, and the sample (purple) in a cuvette (blue) with an expanded image of BR reconstituted into DSPC-d_{70} lipids. Transients of the single wavenumber measurements are acquired with two channels covering different time frames ranging from 100 ns to 20 ms. A more detailed sketch is shown in Fig. S1 of the supplementary material.

deprotonated Schiff base, it is considered the key intermediate for the proton transport.[16] The finishing steps in the photocycle are the thermal reisomerization and the reset of the Schiff base accessibility.

The photocycle intermediates were extensively studied and characterized by Fourier-transform infrared (FTIR) difference spectroscopy, which is a suitable tool for the investigation of protein reactions.[15] In contrast to IR absorption spectroscopy, only those vibrational modes are detected, which change during the reaction. An appropriate method for highly repetitive systems and nanosecond time resolution is step-scan FTIR.[17] For this technique, the movable mirror of the FTIR spectrometer is stopped and moved further in a step-wise manner. At each position, the reaction is triggered and the resulting signal is detected along the time axis. After measurements at all mirror positions, the data are merged into interferograms and processed.[11] The time resolution is limited by the rise time of the detector, the sampling speed of the analog-to-digital converter, and its memory capacity. The spectral resolution is dependent on the number of mirror positions.[15]

One approach to gain insights into the protein-membrane interplay is to analyze the impact on the protein reaction upon changing the membrane environment. In our previous step-scan FTIR studies, BR was reconstituted into artificial membranes with a systematic variation of the lipid properties, such as head group charge, lipid chain length, and lipid chain saturation. The effect of the membrane composition on the proton transfer and conformational changes could be disassembled.[18,19] The protonation dynamics have been found to be significantly affected by the variation of the lipid head group charge, while bilayer thickness defined by the lipid chain length had only a minor influence. However, the degree of lipid saturation had superior influence. In these FTIR studies, we probed the protein vibrational modes to evaluate the effect of the lipid environment on protein dynamics. We could not resolve changes in the lipid vibrational modes because the FTIR method reached its limits. It should be noted that the spectral changes in the difference spectra are expected to be very small as only lipids contribute, which are located at the membrane–protein interface and interact with the protein.

By the introduction of quantum cascade lasers (QCLs),[20] an IR source superior in spectral brilliance compared to FTIR[21,22] was provided with application in diverse scientific branches.[23–26] Signal-to-noise ratio advantages in mid-infrared transmission spectroscopy of proteins compared to FTIR spectroscopy were achieved.[27] More recently, various forms of QCL setups for the investigation of BR were presented, and the successful application of time-resolved single wavenumber measurements at various precisely selected IR bands has been reported.[28–31] Our home-built QCL spectrometer with multiple laser heads provides a nearly gapless tunability in a broad spectral region from around 1150 cm^{-1} up to 2250 cm^{-1} (Fig. 1). BR proton transfer kinetics as well as protein conformational dynamics have been measured before.[30] Here, the investigated spectral region will be expanded to ~2000 to 2300 cm^{-1} in order to analyze lipid vibrational modes.

As the membrane model system, we chose 1,2-distearoyl-sn-*glycero*-3-phosphocholine (DSPC) proteoliposomes. The protonation dynamics of BR in DSPC are similar compared to BR in the native purple membrane.[18] DSPC is a lipid with 18 carbon long saturated alkyl chains and neutral head groups, whereas the native purple membrane consists mainly of lipids with 16 carbon long alkyl chains, but also saturated, and a negative charge of the lipid head group.[7,32] The measurements were performed at 20 °C, below the phase transition temperature of DSPC (55 °C)[33] and purple membrane (>70 °C).[34] To avoid overlapping IR bands of the membrane's lipid alkyl chains with water as well as interfering artifacts originating from heating effects of the water by the pump pulse,[35,36] the photoreceptor was reconstituted into liposomes with fully deuterated tails [Fig. 1(a), bottom]. The vibrational modes of the deuterated lipid alkyl chains shift into a spectral silent window with very minor water contributions[37] and are in the coverage area of our QCLs. The observable lipid chain dynamics result only from those lipids close to the protein interface, which are affected by the light-triggered changes of the protein. Most lipids of the bulk membrane do not react to photo-excitation. Thereby, our previous studies monitoring the membrane effects by the protein reaction are expanded to investigations of dynamics of the membrane environment itself.

MATERIAL AND METHODS

Sample preparation

The purple membrane was isolated and purified from *Halobacterium salinarium* as described by Oesterhelt and Stoeckenius.[38] From the purified purple membrane, BR was solubilized using 0.8% Triton X-100 and 50 mM phosphate buffer (pH 7). Lipids of DSPC (1,2-distearoyl-sn-*glycero*-3-phosphocholine, Avanti Polar Lipids) and DSPC-d_{70} (1,2-distearoyl-d70-sn-*glycero*-3-phosphocholine, Avanti Polar Lipids) were dissolved in chloroform ($CHCl_3$) and lyophilized. The lipids were rehydrated in Tris-HCL (pH 7.4) to a concentration of 5 mg/ml. Subsequent to sonification, the liposomes were extruded using a 100 nm pore size filter and mixed with solubilized BR in a lipid-to-protein ratio of 2:1 (w/w). By removing the detergent using detergent adsorbing beads (SM2 Bio-Beads, Bio-Rad) followed by centrifugation at 100 000 g for 1 h at 4 °C, the proteoliposomes were received.

The same sample preparation was used for FTIR- and QCL-measurements. About 140 μg of BR proteoliposomes, respectively, BR in the purple membrane for reference measurements, were dried as a film under constantly flowing nitrogen on a calcium fluoride thin cuvette with a 10 μm optical path length. The film was rehydrated with 1 μl of ultra-pure water. A calcium fluoride window sealed the cuvette and prevents dehydration. Sample preparation was well reproducible with respect to the hydration degree and lipid-to-protein ratio as verified in the absorption spectra of separately prepared samples.

Kinetic data of reconstituted BR in DSPC, respectively, DSPC-d_{70}, are averaged of measurements with two separately prepared samples each to ensure reproducibility. Before data were acquired, the samples were light-adapted with laser pulses.

FTIR spectroscopy

FTIR absorption spectra (Fig. 2) were recorded with a spectral resolution of 4 cm^{-1} (Equinox 55, Bruker). Time-resolved FTIR spectra [Figs. 4(a) and 4(b)] were performed with the step-scan technique (Vertex 80v, Bruker). The time resolution was set to 10 μs, and spectra were recorded from 10 μs to 19 ms with a spectral resolution of 8 cm^{-1} and 2000 mirror positions. Subsequently, the transients were extracted at the desired wavenumbers from the spectra.

QCL spectrometer setup

The home-built QCL spectrometer setup is shown in a simplified version in Fig. 1 and more detailed in Fig. S1 of the supplementary material. Four different external cavity QCL laser heads (QCL 1–4, MIRcat-QT, DRS-Daylight Solutions, Inc.) were built within the laser source, providing gapless tuning between 1475 and 2250 cm^{-1} (QCL 1: 1950–2250 cm^{-1}; QCL 2: 1650–1950 cm^{-1}; and QCL 3: 1475–1750 cm^{-1}) and from 1150 to 1350 cm^{-1} (QCL 4). For measurements in transmission, the probe beam was focused

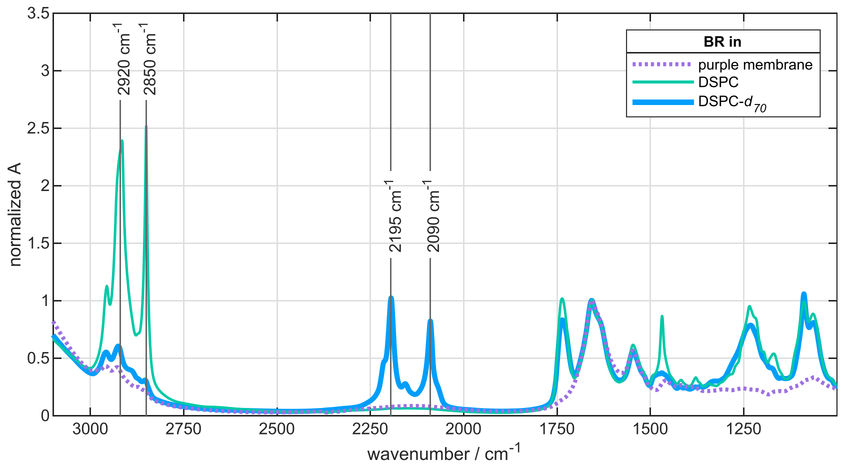

FIG. 2. FTIR absorption spectra of BR in the purple membrane (purple), reconstituted into DSPC lipids (green) and DSPC-d_{70} lipids with fully deuterated lipid chains (blue). The bands at ~2850 and ~2920 cm^{-1} mainly originate from the symmetric and antisymmetric CH_2 stretching modes of the DSPC alkyl lipid chains. Deuteration shifts the lipid chain bands to 2090 and 2195 cm^{-1}, which are the symmetric and antisymmetric stretching modes of CD_2.

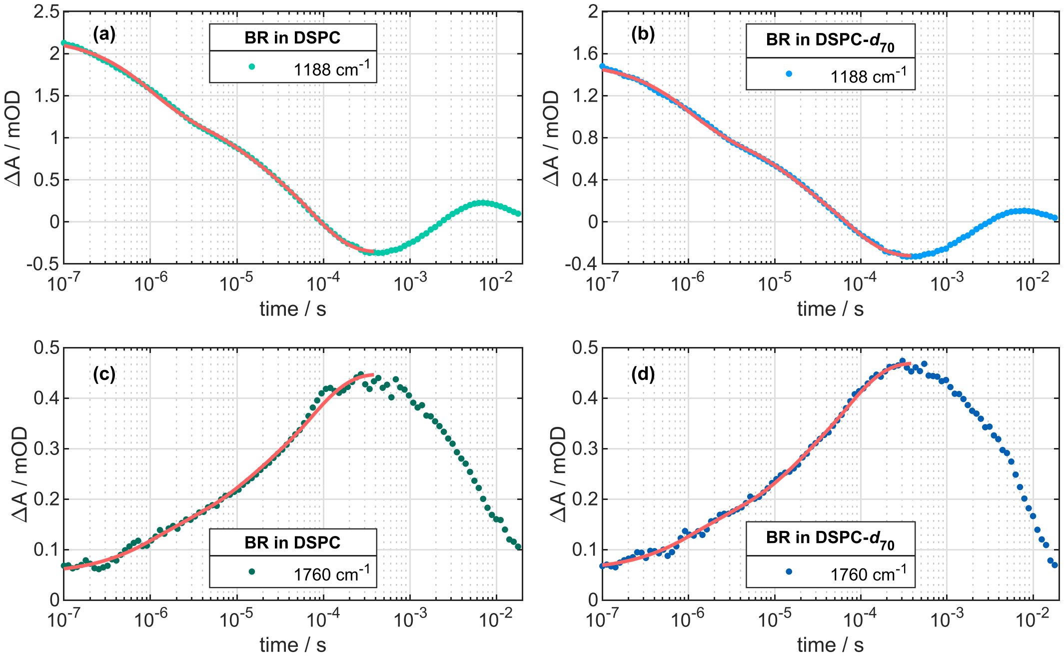

FIG. 3. Time-depended QCL measurements at single wavenumbers. De- and reprotonation dynamics of the Schiff base monitored at 1188 cm^{-1} for BR in (a) DSPC and (b) deuterated DSPC-d_{70}. Protonation dynamics of the primary proton acceptor Asp85 observed at 1760 cm^{-1} for BR in (c) DSPC and (d) deuterated DSPC-d_{70}. The data fits (red lines) until ∼430 μs show the coincidence of the deprotonation dynamics of the Schiff base with the protonation dynamics of Asp85.

(f = 152.4 mm) onto the sample and collimated afterward (f = 101.6 mm) with a pair of off-axis parabolic mirrors (OAPs). Another OAP with a focal length of 76.2 mm focused the beam onto the mercury cadmium telluride (MCT) detector (Kolmar Technologies, Inc.). A polarizer and analyzer were used to control the power at the detector. A long-pass filter and a band-pass filter matching the probe wavenumber were attached light-tightly to the detector to avoid interfering signals. The spectrometer setup was continuously flushed with dried air, and the sample cuvette was maintained at a constant temperature of 20 °C. The photoexcitation was initiated by 5 ns laser pulses of the second harmonic (532 nm) of a Q-switched Nd:YAG laser (Minilite, Continuum Electro-Optics, Inc.). Through the widening of the pump beam by a pair of concave (f = −50 mm) and convex (f = 200 mm) lenses and subsequently trimming with a 2 mm pinhole, a spatially more homogeneous excitation of the probed area is achieved. Moreover, this defined beam diameter was used for setting the excitation energy density to 2 mJ cm^{-2}. The data were recorded using three channels from two 16-bit transient recorder boards (M3i.4841/M2p.5960-x4, Spectrum Instrumentation). For data acquisition over five decades, from 100 ns to 20 ms, the time trace was split before and after at 1 ms to different transient recorder boards operating at different sampling rates. The board covering the faster dynamics from 100 ns to 1 ms was set to 125 MS s^{-1}, while the second board was set to 10 MS s^{-1} to collect data until 20 ms. The 16-bit resolution is distributed to ±200 mV of the recorded AC-data. The third channel was used for the associated DC value. 2000 transients were averaged. The data collection as well as the remote control of the setup was realized through self-written Matlab programs (Version 9.11.0, Mathworks Inc). A signal with a blocked pump beam was measured as a reference.

Data analysis

The absorbance difference was calculated by $\Delta A(t) = -\log_{10}(I(t)/I(t)_{\mathrm{ref}})$, where $I(t)$ is the time-dependent voltage recorded at the detector and corrected by the separately measured DC offset. The reference signal $I(t)_{\mathrm{ref}}$ is acquired with a dark-state sample and determined equivalently. The resulting transients were logarithmically averaged at 20 points per decade. The data processing was performed with Matlab (Version 9.9.0, Mathworks Inc.). For determination of the time constants τ, the logarithmically

TABLE I. Shared time constants of the first proton transfer step for BR in the purple membrane, reconstituted into DSPC and DSPC-d_{70} derived from fitting analysis of single wavenumber measurements at 1188 cm^{-1} (Schiff base deprotonation) and 1760 cm^{-1} (Asp85 protonation).[a]

BR in	$\tau_{\mathrm{sh},1}^{\mathrm{BR}}$ (μs)	$\tau_{\mathrm{sh},2}^{\mathrm{BR}}$ (μs)	$\tau_{\mathrm{sh},3}^{\mathrm{BR}}$ (μs)
Purple membrane	0.94 ± 0.03	11.22 ± 1.00	72.00 ± 2.82
DSPC	0.91 ± 0.03	8.23 ± 0.79	74.07 ± 1.93
DSPC-d_{70}	0.94 ± 0.03	9.99 ± 0.91	70.96 ± 2.30

[a] Standard error from the fitting routine.

averaged data were fitted with exponential functions $\mathrm{f}(t)$ with m terms iterated with n,

$$\mathrm{f}(t) = c_0 + \sum_{n=1}^{m} A_n \times \exp\left(-\frac{t}{\tau_n}\right), \tag{1}$$

where t is time, A_n is the amplitude, and c_0 is the y-axis offset. Moreover, a variation of this function was used for the evaluation of two interdependent transients,

$$\begin{pmatrix} \mathrm{f}^1_{\mathrm{sh}}(t) \\ \mathrm{f}^2_{\mathrm{sh}}(t) \end{pmatrix} = \begin{pmatrix} c^1_0 \\ c^2_0 \end{pmatrix} + \sum_{n=1}^{m} \begin{pmatrix} A^1_n \\ A^2_n \end{pmatrix} \times \exp\left(-\frac{t}{\tau^{\mathrm{BR}}_{\mathrm{sh},n}}\right), \tag{2}$$

where τ_{sh} is a shared time constant to both recorded signals, but the amplitude A_n and the offset c_0 are independent. The number of time constants (respectively, number of terms m) was chosen to result in the best fit with the minimum number of exponential components. For the protonation and deprotonation dynamics of BR with the functions $\mathrm{f}^{1188}_{\mathrm{sh}}(t)$ and $\mathrm{f}^{1760}_{\mathrm{sh}}(t)$, three exponential components were used in a time window up to ~430 μs,

$$\begin{pmatrix} \mathrm{f}^{1188}_{\mathrm{sh}}(t) \\ \mathrm{f}^{1760}_{\mathrm{sh}}(t) \end{pmatrix} = \begin{pmatrix} c^{1188}_0 \\ c^{1760}_0 \end{pmatrix} + \begin{pmatrix} A^{1188}_1 \\ A^{1760}_1 \end{pmatrix} \times \exp\left(-\frac{t}{\tau^{\mathrm{BR}}_{\mathrm{sh},1}}\right) + \begin{pmatrix} A^{1188}_2 \\ A^{1760}_2 \end{pmatrix} \times \exp\left(-\frac{t}{\tau^{\mathrm{BR}}_{\mathrm{sh},2}}\right) + \begin{pmatrix} A^{1188}_3 \\ A^{1760}_3 \end{pmatrix} \times \exp\left(-\frac{t}{\tau^{\mathrm{BR}}_{\mathrm{sh},3}}\right). \tag{3}$$

Fits are shown in Figs. 3 and S2 (supplementary material). Resulting time constants are in Table I. For the lipid dynamics, Eq. (1) was applied to the data shown in Fig. 5 to determine the number of components needed. This resulted in three components for 2190 cm^{-1} and four components for 2090 cm^{-1}. The corresponding Eqs. (S1) and (S2) and the time constants in Tables S1 and S2 are shown in the supplementary material and are discussed in the section titled "Results and Discussion." Thereafter, the time constants for the data in Fig. 5 were also determined with shared time constants by using the fitting functions $\mathrm{f}^{2090}_{\mathrm{sh}}(t)$ and $\mathrm{f}^{2190}_{\mathrm{sh}}(t)$ based on Eq. (2). With the obtained result, $\mathrm{f}^{2090}_{\mathrm{sh}}(t)$ contains four exponential components, while $\mathrm{f}^{2190}_{\mathrm{sh}}(t)$ has three by setting the amplitude $A^{2190}_0 = 0$,

$$\begin{pmatrix} \mathrm{f}^{2090}_{\mathrm{sh}}(t) \\ \mathrm{f}^{2190}_{\mathrm{sh}}(t) \end{pmatrix} = \begin{pmatrix} c^{2090}_0 \\ c^{2190}_0 \end{pmatrix} + \begin{pmatrix} A^{2090}_0 \\ 0 \end{pmatrix} \times \exp\left(-\frac{t}{\tau^{\mathrm{lip}}_0}\right) + \begin{pmatrix} A^{2090}_1 \\ A^{2190}_1 \end{pmatrix} \times \exp\left(-\frac{t}{\tau^{\mathrm{lip}}_{\mathrm{sh},1}}\right) + \begin{pmatrix} A^{2090}_2 \\ A^{2190}_2 \end{pmatrix} \times \exp\left(-\frac{t}{\tau^{\mathrm{lip}}_{\mathrm{sh},2}}\right) + \begin{pmatrix} A^{2090}_3 \\ A^{2190}_3 \end{pmatrix} \times \exp\left(-\frac{t}{\tau^{\mathrm{lip}}_{\mathrm{sh},3}}\right), \tag{4}$$

where τ^{lip}_0 is a time constant belonging exclusively to 2090 cm^{-1} and $\tau^{\mathrm{lip}}_{\mathrm{sh},n}$ (with $n = 1, 2, 3$) are the shared time constants of both wavenumbers. Fits are shown in Fig. 5 and the resulting time constants in Table II. For the fitting procedure, Origin (Version 2022, OriginLab Corporation) was used.

RESULTS AND DISCUSSION

Absorption spectra of BR reconstituted into DSPC and DSPC-d_{70} as well as of BR in the native purple membrane are shown in Fig. 2. The spectra are normalized to the amide I band (1600–1700 cm^{-1}).[39] Amide I and amide II (1510–1580 cm^{-1}) bands are caused by the protein backbone vibrations. Lipid bands can be observed in the spectral regions from 1000 to 1800 cm^{-1} and between 2800 and 3000 cm^{-1}, respectively, 2050 and 2250 cm^{-1}, for deuterated lipids. The C=O stretch of the lipid ester group (~1736 cm^{-1}) and amide I (~1656 cm^{-1}) are used to determine the lipid-to-protein ratio in the proteoliposomes for DSPC and DSPC-d_{70}. A slightly weaker lipid band of DSPC-d_{70} indicates a smaller ratio for deuterated than non-deuterated lipids. The broad water band (~3400 cm^{-1}) overlaps with the CH_2 and CH_3 stretching modes of the non-deuterated lipids. The two dominant peaks at ~2850 and ~2920 cm^{-1} are associated with the symmetric and the antisymmetric CH_2 stretching mode.[39] These bands are mainly caused by the alkyl lipid chains but also from CH_2 vibrations of the lipid head groups. It should be noted that the native purple membrane shows only a weak lipid absorption compared to the DSPC and DSPC-d_{70} proteoliposomes due to the significantly different lipid-to-protein ratio.[38]

DSPC-d_{70} differs from DSPC only in fully deuterated lipid chains. Hence, all 70 hydrogen atoms of the alkyl chain were replaced by deuterium. Thus, the absorption spectrum of BR in DSPC-d_{70} shows a strong decline of the CH_2 stretching bands. The signal is not completely vanished due to CH_2 modes of the lipid head groups, not fully removed purple membrane or side-chain contributions. The frequency-shifted peaks linked to the symmetric (~2090 cm^{-1}) and antisymmetric (~2195 cm^{-1}) CD_2 stretching modes[40] now appear in a spectral silent window with only minor interfering water bands.[37] The band intensities of the deuterated lipids are weaker compared to the non-deuterated lipids. We attribute this observation mainly to the significantly weaker underlying water absorption and the missing contribution of the CH_2 vibrations of the head groups.

Protonation dynamics

The protonation dynamics of BR reconstituted into DSPC [Figs. 3(a) and 3(c)] and BR reconstituted into DSPC-d_{70} [Figs. 3(b) and 3(d)] were investigated and compared to BR in the purple membrane (Fig. S2, supplementary material). The first step of the proton translocation is the deprotonation of the Schiff base, which can be monitored at 1188 cm^{-1} [Figs. 3(a) and 3(b)].[10] This deprotonation results in a steady decline of the absorbance change to a minimum at ~400 μs corresponding to the M intermediate. After reprotonation of the Schiff base and relaxation of BR to the ground state, the transient converges toward zero. This kinetic trace represents the rise and decay of the M intermediate and relaxation toward the ground state as the band at 1188 cm^{-1} is assigned to the C–C stretch of the 13-*cis* retinal, which is sensitive to the protonation state of the Schiff base. Asp85 is the primary proton acceptor of the proton from the Schiff base. Thus, coincidently with the deprotonation of the Schiff base, the protonation dynamics of Asp85 can be observed by an increasing absorbance change at 1760 cm^{-1} [Figs. 3(c) and

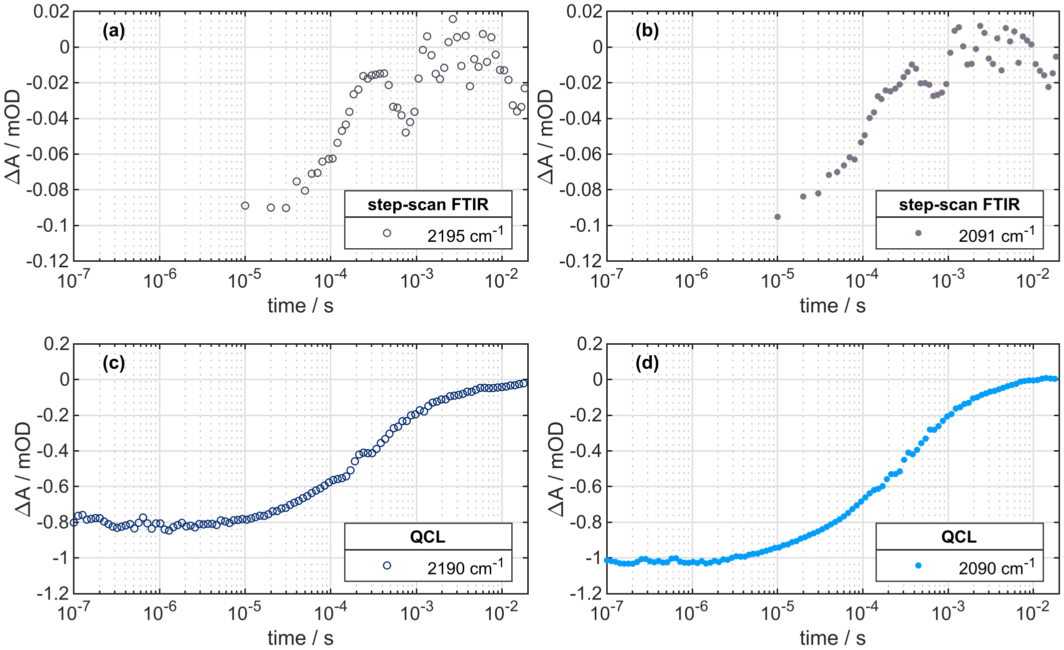

FIG. 4. Detection of lipid dynamics (CD_2 stretching vibrations) with step-scan FTIR at (a) 2195 cm^{-1} and (b) 2091 cm^{-1} and with QCL measurements (c) at 2190 cm^{-1} and (d) 2090 cm^{-1}. Note the difference of a factor of 10 on the y-axis scale between FTIR- and QCL-measurements.

3(d)].[41] While Asp85 remains protonated in the N and O intermediates, the observation thereof shifts to lower wavenumbers, and in combination with the BR recovery, this band relaxes again. However, at ~1760 cm^{-1}, after passing its maximum at ~400 μs, the decrease in the kinetic trace is in good agreement with the decaying M intermediate.[10]

We compared the M intermediate kinetics to evaluate if the DSPC and DSPC-d_{70} lipids provide similar environments and interactions with BR compared to the native purple membrane. We could not apply a global fit analysis because single wavenumber measurements do not provide whole spectra. With only two, but directly related transients at 1188 and 1760 cm^{-1}, we evaluated the data by a fit that includes shared time constants τ_{sh}^{BR} and independent amplitudes. The fitting function is based on Eq. (2) and includes a sum of three exponentials in the fitted time window from 100 ns to ~430 μs [Eq. (3)]. The resulting time constants for BR in the purple membrane, in DSPC, and in DSPC-d_{70} are shown in Table I.

The time constants of BR in the purple membrane derived from our measurements and analyzed as described above were compared with other published data (Table S3, supplementary material). The fastest time constant $\tau_{sh,1}^{BR}$ is ~1 μs. Nanosecond step-scan FTIR data yielded time constants of 0.78[42] and 1.2 μs,[43] and other single wavenumber QCL (SW-QCL) measurements recorded in the spectral range from 1700 to 1800 cm^{-1}, provided time constants of 0.4 and 1.2 μs.[22] The second time constant $\tau_{sh,2}^{BR}$ ~11 μs is also in good agreement with other studies. 8 μs[22] were determined by SW-QCL and 12 μs[29] by dual frequency comb QCL spectroscopy (DCS-QCL) recorded in a spectral range from 1185 to 1240 cm^{-1}. Step-scan FTIR studies lead to slightly higher time constants of 18[29] and 22 μs.[43] The third time constant $\tau_{sh,3}^{BR}$ of 72 μs also matches well with a SW-QCL study, yielding 75 μs[22] and also with 74 μs[18] found in our previous study performed with step-scan FTIR and analyzed by a global fit. DCS-QCL measurements result in 56.3[31] and 65.3 μs[31] as well as 140 μs.[29] Step-scan measurements in the literature lead to slightly higher time constants of 78,[44] 122,[29] 130,[43] and 134 μs.[42] Overall, there is consistency, especially if one considers the different spectral and time ranges, but also minor measurement condition differences in pH and a certain deviation of temperatures. This demonstrates that the reproduction of the time constants based on two selected single wavenumbers, 1188 and 1760 cm^{-1}, provides consistent results.

BR reconstituted into DSPC liposomes reveals similar three time constants with ~1, ~8, and ~74 μs for DSPC compared to ~1, ~11, and 72 μs for the purple membrane and agrees well with previous steps-scan data and global fit analysis.[18] Therefore, BR reconstituted into DSPC is an appropriate model system for the purple membrane. BR reconstituted into DSPC-d_{70} liposomes shows time constants of ~1, ~10, and ~71 μs. Hence, the deuteration of the lipid chains is not affecting the dynamics.

Lipid dynamics detected by step-scan FTIR and SW-QCL

Our first approach to monitor directly the lipid vibrations for investigating the interplay of the protein and its surrounding membrane was done with step-scan FTIR. The maximum absorbance changes of the CD_2 stretching vibrations occur at

2195 and 2091 cm^{-1}, and the transients were extracted from the FTIR spectra [Figs. 4(a) and 4(b)]. The absorbance changes are relatively small, as expected because only those lipids contribute to the signal, which interact with the protein during the photoreaction, whereas most of the lipids in the bulk membrane will not be involved. Both transients indicate the existence of lipid chain dynamics; however, the signal quality was not sufficient for further analysis. Using the same sample preparation, we measured the lipid vibrations with our QCL setup [Figs. 4(c) and 4(d)]. Since the nominal edge of the QCL emission spectrum at 2250 cm^{-1} is shifted due to the losses by the spectrometer optics, e.g. the polarizers, the most suitable wavenumber to measure the dynamics was 2190 cm^{-1}, which is slightly lower than 2195 cm^{-1}. Remarkable is the extension of the time range along the x-axis, especially in combination with the improvement in the resolution of the signal in the y-direction. Qualitatively, the FTIR- and QCL-measurements indicate the same trend as both transients start from a negative absorbance value and then relax toward zero again. Photothermally induced water dynamics of BR have been reported previously in the here studied spectral region[36] since the bend + libration water combination band absorbs around 2130 cm^{-1}.[37] We can exclude significant contributions of photothermally heated water interfering with the CD_2 lipid dynamics by control measurements (Fig. S3, supplementary material).

Comparing step-scan FTIR- and QCL-data from Fig. 4, the most notable difference is the magnitude of the observed absorbance change being about ten times larger for the QCL measurements. The QCL probe beam has a spectral brightness many orders of magnitude higher than the polychromatic IR source used in FTIR.[21] Thus, the signal-to-noise ratio is much better in SW-QCL measurements, which becomes particularly apparent when small absorbance changes are monitored. The total absorbance change in the FTIR data is less than 0.1 mOD, and the scattering of the data points is obvious. The significant difference in absorbance change may be attributable to inhomogeneities of the BR film in combination with different sizes of probed areas. The diameter of the FTIR probe beam is a few millimeters, while the QCL beam is in the range of hundreds of micrometers. This can result in a higher local concentration in QCL-probed measurements compared to FTIR-detected measurements. The different probe spot sizes have further consequences for the photoexcitation of the pump laser's Gaussian beam profile. The diameter of the pump beam is similar to the size of the FTIR probe beam. Since the QCL probe spot is manifold smaller, it is located in the inner center of the pump beam. Thereby, an effectively higher power density excites the probed intersection on the sample. Additionally, a proportionally small and centrally located probe spot provides a more homogeneous excitation. In contrast to the edges of the Gaussian intensity distribution, no significant change in intensity is in its center. Therefore, a more defined excitation energy can be adjusted and enables a higher comparability of experiments. Besides the fundamentally different ways of data acquisition and processing of FTIR and QCL spectrometers, the spectral resolution differs between the two measurement techniques. While SW-QCL measurements provide an extremely narrow linewidth (<100 MHz), the measured transients are more independent from nearby bands. With a typical spectral resolution of 8 cm^{-1} in step-scan FTIR,[15] both the time trace and the absorbance change within this range could interdependently influence the result. Distorting effects of insufficient temporal resolution or strong noise also lead to varying outcomes. Other studies also show variances in the signal extracted from step-scan FTIR and measured with single wavenumber QCLs.[22,45]

Correlation of lipid chain and BR protonation dynamics

For a more detailed analysis of lipid dynamics, the transients of the deuterated lipid chains [Figs. 4(c) and 4(d)] were normalized and are shown in Fig. 5. With this representation, the matching of the transients at t > 200 μs and also the deviation around 10 μs become visible.

Reproducing the more than five-decade spanning time trace, a minimum of three exponential components is necessary. Therefore, Eq. (S1) of the supplementary material based on Eq. (1) with a sum of three independent exponentials was selected. The fitting results for the time constants are shown in Table S1 of the supplementary material. For both transients, the three time constants describing the lipid dynamics occur in the same orders of magnitude, $\tau_1^{\text{lip},3}$ in tens of microseconds, $\tau_2^{\text{lip},3}$ in some hundreds of microsecond, and $\tau_3^{\text{lip},3}$ in a few milliseconds. The time constants were compared with the time constant of the protonation dynamics of the protein (Table I). Time constant $\tau_1^{\text{lip},3}$ measured at 2190 cm^{-1} (68 μs) matches to time constant $\tau_{\text{sh},3}^{\text{BR}}$ monitored at 1188 and 1760 cm^{-1} (71 μs). The deviation of the two lipid transients observed around 10 μs (Fig. 5) is reflected by the faster relaxation at 2090 cm^{-1} with $\tau_1^{\text{lip},3}$ = 30 μs. Regarding

TABLE II. Shared time constants and relative amplitudes of the lipid chain dynamics at 2090 and 2190 cm^{-1} from Fig. 5 using Eq. (4).[a]

BR in DSPC-d_{70}	τ_0^{lip} (μs)	A_0 (%)	$\tau_{\text{sh},1}^{\text{lip}}$ (μs)	A_1 (%)	$\tau_{\text{sh},2}^{\text{lip}}$ (μs)	A_2 (%)	$\tau_{\text{sh},3}^{\text{lip}}$ (μs)	A_3 (%)
2090 cm^{-1}	13 ± 4	8	68 ± 10	18	440 ± 41	54	3095 ± 520	20
2190 cm^{-1}	⋯	0		23		57		19

[a] Standard error from the fitting routine.

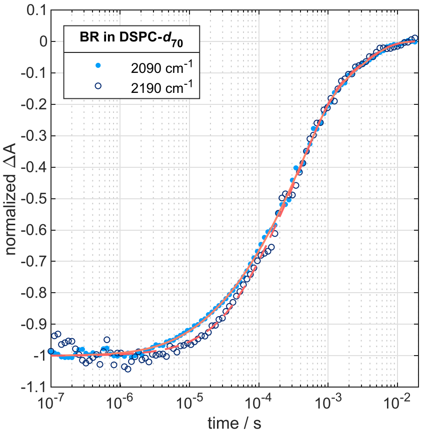

FIG. 5. Normalized QCL measurements of deuterated lipid chain dynamics at 2190 cm^{-1} (open circles) and 2090 cm^{-1} (filled dots). The fits (red) were performed with Eq. (4), and the derived time constants are in Table II. The transients are linked to the antisymmetric and symmetric stretching of CD_2.

the slower time constant, $\tau_2^{\text{lip},3}$ of ~370 μs (2090 cm^{-1}) and ~430 μs (2190 cm^{-1}) as well as $\tau_3^{\text{lip},3}$ of ~2.7 ms (2090 cm^{-1}) and ~2.9 ms (2190 cm^{-1}), the well matching time constants support the matching course of the transients. To explore if the use of more than three time constants change the result, an extra exponential was added to the fit by applying Eq. (S2) of the supplementary material. While the fit for the lipid chain dynamics at 2190 cm^{-1} is not improving, an additional exponential component provides a better fitting result for 2090 cm^{-1}. The resulting time constants for 2090 cm^{-1} are 11 μs ($\tau_0^{\text{lip},4}$), 58 μs ($\tau_1^{\text{lip},4}$), 431 μs ($\tau_2^{\text{lip},4}$), and 3.1 ms ($\tau_3^{\text{lip},4}$) and shown in Table S2 of the supplementary material. Five components did not improve the fits as opposed to four. Besides optimizing the fits for the transients at 2090 and 2190 cm^{-1} individually, the same concept of shared time constants was performed for the lipid dynamics as done above for the protonation dynamics of BR. This results in an equation with three shared exponentials but one independent additional for 2090 cm^{-1} [Eq. (4)]. The determined time constants are shown in Table II.

With this approach, the lipid transients are well described by the fit functions shown in Fig. 5. Lipid and BR protonation dynamics of the M intermediate (Table I) have been compared. The fastest time constant $\tau_{\text{sh},1}^{\text{BR}}$ (1 μs) has no counterpart, but $\tau_{\text{sh},2}^{\text{BR}}$ (10 μs) correlates with τ_0^{lip} (13 μs) and $\tau_{\text{sh},3}^{\text{BR}}$ (71 μs) with $\tau_{\text{sh},1}^{\text{lip}}$ (68 μs). Time constants of 300,[46] 469,[13] and 544 μs[42] have been reported for BR and $\tau_{\text{sh},2}^{\text{lip}}$ (440 μs) is found in the same time domain. Likewise, $\tau_{\text{sh},3}^{\text{lip}}$ (3.1 ms) matches with time constants of 2.6,[43] 2.8,[31] 3,[46] 3.01,[31] and 3.3 ms.[29] The fact that every time constant finds its counterparts implies that the detected lipid dynamics are linked to the protein's photocycle. Control measurements also indicate that lipid dynamics are induced by the protein activity since the laser excitation of just DSCP-d_{70} liposomes without protein has no effect on the vibrational modes of the bulk lipids (Fig. S3 of the supplementary material). The amplitudes of the fits give the largest fraction at $\tau_{\text{sh},2}^{\text{lip}}$ with 440 μs, which corresponds to the decay of the M intermediate detectable at the minimum of Fig. 3(b), and also found in other studies about 300–400 μs after photoexcitation.[14,15] Since the protonation dynamics correlate with conformational changes,[18] this could hint at a strong link between lipid dynamics and large-scale conformational changes of the M intermediate. The kinetics of the symmetric and antisymmetric stretching vibrations are expected to be similar; however, the deviation at 10 μs is reproducible and the reason remains to be clarified. For further conclusions, more data from measurements at specifically selected wavenumbers are needed. As the transients have to be measured individually, a dataset composed of all the necessary wavenumbers to map each kinetic resolving all intermediates would be desirable to link lipid dynamics to the photocycle.

CONCLUSIONS

DSPC proteoliposomes serve as a suitable model for a membrane environment of BR. This is supported by similar time constants for the protonation dynamics of the M intermediate measured for BR in the native purple membrane. Furthermore, the deuteration of the lipid chains does not affect the kinetics. Measurements with our home-built QCL spectrometer enabled the observation of lipid chain dynamics in a time window from 100 ns to 20 ms. The resolved lipid dynamics demonstrate the improvement of signal-to-noise and better time resolution of single wavenumber QCL over FTIR step-scan measurements. This opens up the field of investigation from the protein's photocycle to lipid-mediated dynamics of the membrane. Hereby, deeper insights into protein–membrane interactions can be gained. The observed symmetric and antisymmetric CD_2 stretching modes of the lipid alkyl chains show a negative absorbance change and subsequent relaxation path, similar for both with only a minor deviation around 10 μs. Correlations between the time constants of the resolved lipid transients and the protonation dynamics of the protein were identified. The evaluation of the single wavenumber data with shared time constants follows the same principle as a global fit analysis of FTIR data, namely, to correlate spectral changes and to identify intermediate states during the photocycle. For the identification of membrane states and correlation with the protein's protonation and conformational change, an extension to additional selected wavenumbers representing other photointermediates is required. Covering the whole photocycle dynamics at characteristic wavenumbers in combination with data evaluation using interdependent time constants for individually measured transients is an aspired objective. Furthermore, detailed molecular analysis of lipid–protein interactions and dynamics becomes feasible with the here presented setup and will be addressed in the future for other membrane proteins.

SUPPLEMENTARY MATERIAL

The supplementary material is provided with a detailed scheme of the experimental setup, time constants of lipid dynamics determined by multiexponential fits, transients and fits of BR in the purple membrane, control measurements on photothermally induced dynamics, and a summary of time constants of the BR photocycle deduced from the literature.

ACKNOWLEDGMENTS

The authors thank Jessica Dröden for the expression and purification of BR. Financial support by the Deutsche Forschungsgemeinschaft (SFB 969, project A2) is gratefully acknowledged.

AUTHOR DECLARATIONS

Conflict of Interest

The authors have no conflicts to disclose.

Author Contributions

Paul Stritt: Data curation (equal); Formal analysis (equal); Investigation (equal); Writing – original draft (equal). **Michael Jawurek**: Investigation (equal). **Karin Hauser**: Conceptualization (equal); Funding acquisition (equal); Writing – review & editing (equal).

DATA AVAILABILITY

The data that support the findings of this study are available within the article and its supplementary material.

REFERENCES

[1] D. Oesterhelt and W. Stoeckenius, Proc. Natl. Acad. Sci. U. S. A. **70**, 2853 (1973).

[2] N. Hasegawa, H. Jonotsuka, K. Miki, and K. Takeda, Sci. Rep. **8**, 13123 (2018).

[3] J. Heberle, Biochim. Biophys. Acta, Bioenerg. **1458**, 135 (2000).

[4] G. Nass Kovacs, J. P. Colletier, M. L. Grunbein, Y. Yang, T. Stensitzki, A. Batyuk, S. Carbajo, R. B. Doak, D. Ehrenberg, L. Foucar, R. Gasper, A. Gorel, M. Hilpert, M. Kloos, J. E. Koglin, J. Reinstein, C. M. Roome, R. Schlesinger, M. Seaberg, R. L. Shoeman, M. Stricker, S. Boutet, S. Haacke, J. Heberle, K. Heyne, T. Domratcheva, T. R. M. Barends, and I. Schlichting, Nat. Commun. **10**, 3177 (2019).

[5] C. Wickstrand, R. Dods, A. Royant, and R. Neutze, Biochim. Biophys. Acta **1850**, 536 (2015).

[6] Y. T. Li, Y. Tian, H. Tian, T. Tu, G. Y. Gou, Q. Wang, Y. C. Qiao, Y. Yang, and T. L. Ren, Sensors **18**, 1368 (2018).

[7] A. Corcelli, V. M. T. Lattanzio, G. Mascolo, P. Papadia, and F. Fanizzi, J. Lipid Res. **43**, 132 (2002).

[8] U. Haupts, J. Tittor, E. Bamberg, and D. Oesterhelt, Biochemistry **36**, 2 (1997).

[9] J. Heberle, J. Fitter, H. J. Sass, and G. Büldt, Biophys. Chem. **85**, 229 (2000).

[10] V. A. Lórenz-Fonfría, H. Kandori, and E. Padrós, J. Phys. Chem. B **115**, 7972 (2011).

[11] I. Radu, M. Schleeger, C. Bolwien, and J. Heberle, Photochem. Photobiol. Sci. **8**, 1517 (2009).

[12] D. Oesterhelt, Curr. Opin. Struct. Biol. **8**, 489 (1998).

[13] R. W. Hendler, C. W. Meuse, M. S. Braiman, P. D. Smith, and J. W. Kakareka, Appl. Spectrosc. **65**, 1029 (2011).

[14] F. Garczarek, L. S. Brown, J. K. Lanyi, and K. Gerwert, Proc. Natl. Acad. Sci. U. S. A. **102**, 3633 (2005).

[15] V. A. Lorenz-Fonfria, Chem. Rev. **120**, 3466 (2020).

[16] J. Tittor, S. Paula, S. Subramaniam, J. Heberle, R. Henderson, and D. Oesterhelt, J. Mol. Biol. **319**, 555 (2002).

[17] W. Uhmann, A. Becker, C. Taran, and F. Siebert, Appl. Spectrosc. **45**, 390 (1991).

[18] M. Jawurek, J. Dröden, B. Peter, C. Glaubitz, and K. Hauser, Chem. Phys. **512**, 53 (2018).

[19] M. Jawurek, C. Glaubitz, and K. Hauser, Biomed. Spectrosc. Imaging **5**, 167 (2016).

[20] J. Faist, F. Capasso, D. L. Sivco, C. Sirtori, A. L. Hutchinson, and A. Y. Cho, Science **264**, 553 (1994).

[21] M. Weida and B. Yee, Proc. SPIE **7902**, 79021C (2011).

[22] B.-J. Schultz, H. Mohrmann, V. A. Lorenz-Fonfria, and J. Heberle, Spectrochim. Acta, Part A **188**, 666 (2018).

[23] H.-W. Siu, B. Heck, M. Kovermann, and K. Hauser, Chem. Sci. **12**, 412 (2021).

[24] M. S. Vitiello, G. Scalari, B. Williams, and P. De Natale, Opt. Express **23**, 5167 (2015).

[25] Y. Yao, A. J. Hoffman, and C. F. Gmachl, Nat. Photonics **6**, 432 (2012).

[26] K. Isensee, N. Kröger-Lui, and W. Petrich, Analyst **143**, 5888 (2018).

[27] A. Schwaighofer, M. Montemurro, S. Freitag, C. Kristament, M. J. Culzoni, and B. Lendl, Anal. Chem. **90**, 7072 (2018).

[28] V. Giliberti, R. Polito, E. Ritter, M. Broser, P. Hegemann, L. Puskar, U. Schade, L. Zanetti-Polzi, I. Daidone, S. Corni, F. Rusconi, P. Biagioni, L. Baldassarre, and M. Ortolani, Nano Lett. **19**, 3104 (2019).

[29] J. L. Klocke, M. Mangold, P. Allmendinger, A. Hugi, M. Geiser, P. Jouy, J. Faist, and T. Kottke, Anal. Chem. **90**, 10494 (2018).

[30] P. Stritt, M. Jawurek, and K. Hauser, Biomed. Spectrosc. Imaging **9**, 55 (2020).

[31] L. Schubert, P. Langner, D. Ehrenberg, V. A. Lorenz-Fonfria, and J. Heberle, J. Chem. Phys. **156**, 204201 (2022).

[32] A. G. Lee, Biochim. Biophys. Acta, Biomembr. **1612**, 1 (2003).

[33] R. Koynova and M. Caffrey, Biochim. Biophys. Acta **1376**, 91 (1998).

[34] M. B. Jackson and J. M. Sturtevant, Biochemistry **17**, 911 (1978).

[35] C. Rödig and F. Siebert, Appl. Spectrosc. **53**, 893 (1999).

[36] F. Garczarek, J. Wang, M. A. El-Sayed, and K. Gerwert, Biophys. J. **87**, 2676 (2004).

[37] P. K. Verma, A. Kundu, M. S. Puretz, C. Dhoonmoon, O. S. Chegwidden, C. H. Londergan, and M. Cho, J. Phys. Chem. B **122**, 2587 (2018).

[38] D. Oesterhelt and W. Stoeckenius, Methods Enzymol. **31**, 667 (1974).

[39] L. K. Tamm and S. A. Tatulian, Q. Rev. Biophys. **30**, 365 (1997).

[40] J. L. R. Arrondo and F. M. Goñi, Chem. Phys. Lipids **96**, 53 (1998).

[41] M. S. Braiman, T. Mogi, T. Marti, L. J. Stern, H. G. Khorana, and K. J. Rothschild, Biochemistry **27**, 8516 (1988).

[42] C. Rödig, I. Chizhov, O. Weidlich, and F. Siebert, Biophys. J. **76**, 2687 (1999).

[43] R. Rammelsberg, G. Huhn, M. Lübben, and K. Gerwert, Biochemistry **37**, 5001 (1998).

[44] V. A. Lórenz-Fonfría and H. Kandori, J. Am. Chem. Soc. **131**, 5891 (2009).

[45] T. Resler, B.-J. Schultz, V. A. Lórenz-Fonfría, R. Schlesinger, and J. Heberle, Biophys. J. **109**, 287 (2015).

[46] V. A. Lórenz-Fonfría, Y. Furutani, and H. Kandori, Biochemistry **47**, 4071 (2008).